Available online at www.sciencedirect.com
ScienceDirect
Journal of Organometallic Chemistry 692 (2007) 2903–2910
Journal of Organometallic Chemistry
www.elsevier.com/locate/jorganchem

Synthesis, molecular, crystal and electronic structure of $[(C_6H_6)RuCl(1,10\text{-}C_{12}H_8N_2)]Cl$

J.G. Małecki [a,*], M. Jaworska [b], R. Kruszynski [c]

[a] Department of Inorganic and Radiation Chemistry, Institute of Chemistry, University of Silesia, 9th Szkolna St., 40–006 Katowice, Poland
[b] Department of Theoretical Chemistry, Institute of Chemistry, University of Silesia, 9th Szkolna St., 40–006 Katowice, Poland
[c] Department of X-ray Crystallography and Crystal Chemistry, Institute of General and Ecological Chemistry, Łódź University of Technology, 116 Żeromski St., 90–924 Łódź, Poland

Received 9 February 2005; received in revised form 9 May 2005; accepted 26 February 2007
Available online 15 March 2007

Abstract

The $[(C_6H_6)RuCl(1,10\text{-}C_{12}H_8N_2)]Cl$ complex has been prepared and studied by IR, UV–Vis, ^1H NMR spectroscopy and X-ray crystallography. The complex was prepared in reaction of $[(C_6H_6)RuCl_2]_2$ with 1,10-phenatroline in acetone. The electronic spectrum of the compound has been calculated using the TDDFT method.

Keywords: Ruthenium arene complexes; Phenanthroline; X-ray structure; Bond valence; TDDFT method

1. Introduction

The η^6-arene ruthenium complexes play a vital role in organometallic chemistry [1a–e]. The arene ruthenium halide compounds, obtained by Winkhaus et al. [2], are key starting materials for the formation of wide range of natural and cationic ligand derivatives [1d,3a–d]. The half-sandwich arene ruthenium complexes may serve as excellent catalyst precursors for hydrogenation [3c,4a–e] and for ring-opening metathesis polymerization [4f]. Recent studies of arene ruthenium complexes have shown that they are found to inhibit cancer cell growth [5a–d].

The density functional theory (DFT) has become a very popular computational method for the calculation of a number of molecular properties [6–10]. Because of its greater computational efficiency, DFT has been applied extensively to inorganic and organometallic complexes [11–15]. The time-dependent generalization of DFT (TDDFT) offered a rigorous route to calculate the dynamic response of the charge density [16–19]. The reliability of TDDFT approach in obtaining accurate predictions of excitation energies and oscillator strengths is well documented. The method has been successfully used to calculate electronic spectra of transition metal complexes with variety of ligands [20–22].

In this paper, we present the synthesis, crystal structure, spectroscopic properties and the electronic structure of a benzene ruthenium(II) complex with 1,10-phenanthroline ligand.

2. Experimental

The starting material $[(C_6H_6)RuCl_2]_2$ was synthesized according to the literature procedure [23]. All other reagents were commercially available and were used without further purification.

2.1. Synthesis of $[(C_6H_6)RuCl(1,10\text{-}C_{12}H_8N_2)_2]Cl \cdot 2H_2O$

A mixture of $[(C_6H_6)RuCl_2]_2$ (0.25 g; 5×10^{-4} mol) and 1,10-phenantroline dihydrate (0.3 g; $1{,}4 \times 10^{-3}$ mol) in acetone (100 cm^{-3}) was refluxed for 4 h, cooled and filtered.

* Corresponding author. Tel./fax: +48 32 255911.
E-mail addresses: gmalecki@us.edu.pl (J.G. Małecki), mj@tc3.ich.us.edu.pl (M. Jaworska), kruszyna@p.lodz.pl (R. Kruszynski).

0022-328X/$ - see front matter © 2007 Elsevier B.V. All rights reserved.
doi:10.1016/j.jorganchem.2007.02.048

The crystals suitable for X-ray crystal analysis grew after the reaction mixture was left overnight. Yield 80%.

IR (KBr): 3059 $\nu_{CH-phen}$; 2993 $\nu_{CH-phenyl}$; 1959, 1879 benzene; 1587 ν_{CN}; 1492 $\delta_{(C-CH\ in\ the\ plane)}$; 1422 $\nu_{C=C}$; 1295 $\delta_{(CH)}$; 1091 $\delta_{(C-CH\ in\ the\ plane)}$; 854 $\delta_{(C-C\ out\ of\ the\ plane)}$; 739 $\delta_{(C-C\ out\ of\ the\ plane)}$; 707 $\delta_{(C-C\ in\ the\ plane)}$; 624 $\nu_{Ph.}$ ^{1}H NMR (δ, $CDCl_3$): 8.42 (dd), 7.74 (dd), 8.32 (dd), 7.93 (s), 6.07 (s, C_6H_6), 1.92 (H_2O). UV–Vis (nm, CH_2Cl_2), ($\log\varepsilon$): 449.4 (1.98), 324.0 (4.88), 265.0 (5.47), 232.6 (5.52), 219.8 (5,30) nm. Anal. Calc. for $C_{18}H_{15}Cl_2N_2O_2Ru$: C, 46.66; H, 3.26; Cl, 15.30; N, 6.05; O, 6.91; Ru, 21.81. Found: C, 46.59; H, 3.25; N, 6.03%.

2.2. Physical measurements

Infrared spectra were recorded on a Nicolet Magna 560 spectrophotometer in the spectral range $4000 \div 400\ cm^{-1}$ with the sample in the form of KBr pellet. Electronic spectra were measured on a Lab Alliance UV–Vis 8500 spectrophotometer in the range of 800–280 nm in deoxygenated dichloromethane solution. Elemental analyses (C, H, N) were performed on a Perkin–Elmer CHN-2400 analyzer. The ^{1}H NMR spectra were recorded on a Bruker DRX-400 spectrometer in $CDCl_3$ solutions.

2.3. DFT calculations

GAUSSIAN03 program [24] was used in the calculations. The geometry optimization was carried out with the DFT method with the use of B3LYP functional [25,26]. The electronic spectrum was calculated using the TDDFT method [17].

The calculation was performed using the DZVP basis set [27] with *f* functions with exponents 1.94722036 and 0.748930908 on ruthenium atom, and polarization and diffuse functions to all other atoms: 6-31+g(2d,p) – chlorine, 6-31+g** – carbon, nitrogen and 6-31g(d,p) on hydrogen atoms.

2.4. Crystal structures determination and refinement

A orange plate crystal of $[(C_6H_6)RuCl(1,10\text{-}C_{12}H_8N_2)_2]Cl \cdot 2H_2O$ was mounted on a KM-4-CCD automatic diffractometer equipped with a CCD detector, and used for data collection. X-ray intensity data were collected with graphite monochromated Mo K_α radiation ($\lambda = 0.71073$ Å) at temperature of 293.0(2) K, with ω scan mode. Sixty-second exposure time was used and all Ewald sphere reflections were collected up to $2\theta = 50.01°$. The unit cell parameters were determined from least-squares refinement of the setting angles of 5660 strongest reflections respectively. Details concerning crystal data and refinement are given in Table 1. Examination of two reference frames monitored after each 20 frames measured showed respectively 0.72% loss of the intensity. During the data reduction, the above decay correction coefficient was taken into account. Lorentz, polarization, and numerical absorption [28] corrections were applied. The structures were solved by direct methods. All the non-hydrogen atoms were refined anisotropically using full-matrix, least-squares technique on F^2. All the hydrogen atoms were found from difference Fourier synthesis after four cycles of anisotropic refinement, and refined as "riding" on the adjacent atom with individual isotropic temperature factor equal 1.2 times the value of equivalent temperature factor of the parent atom. SHELXS97 [29], SHELXL97 [30] and SHELXTL [31] programs were used for all the calculations. Atomic scattering factors were those incorporated in the computer programs.

Table 1
Crystal data and structure refinement details of $[(C_6H_6)RuCl(1,10\text{-}C_{12}H_8N_2)_2]Cl \cdot 2H_2O$

Empirical formula	$C_{18}H_{18}Cl_2N_2O_2Ru$
Formula weight	466.31
Temperature (K)	291(2)
Crystal system	triclinic
Space group	$P\bar{1}$
Unit cell dimensions	
a (Å)	7.1700(8)
b (Å)	10.1400(12)
c (Å)	13.3582(12)
α (°)	76.782(9)
β (°)	79.726(9)
γ (°)	74.234(10)
Volume (Å^3)	902.86(17)
Z	2
D_{calc} (Mg/m^3)	1.715
Absorption coefficient (mm^{-1})	1.178
$F(000)$	468
Crystal dimensions (mm)	$0.37 \times 0.31 \times 0.02$
θ Range for data collection (°)	2.98 to 28.64
Index ranges	$-9 \leqslant h \leqslant 9$
	$-13 \leqslant k$ 13
	$-18 \leqslant l$ 17
Reflections collected	11 499
Independent reflections [R_{int}]	4280 [0.0596]
Data/restraints/parameters	4280/0/227
Goodness-of-fit on F^2	1.090
Final R indices [$I > 2\sigma(I)$]	$R_1 = 0.0413$,
	$wR_2 = 0.0751$
R indices (all data)	$R_1 = 0.0665$,
	$wR_2 = 0.0816$
Largest difference in peak and hole	0.533 and −0.637 e Å^{-3}

3. Results and discussion

Refluxing of the ruthenium(II) benzene complex $[(C_6H_6)\text{-}RuCl_2]_2$ with an excess of phenanthroline in acetone leads to the half-sandwich $[(C_6H_6)RuCl(1,10\text{-}C_{12}H_8N_2)_2]Cl$ complex in high yield. The elemental analysis of the complex is in good agreement with their formulation. The characteristic bands of the phenanthroline ligand ν(CN) at 1516 cm^{-1}and ν(C=C) at 1422 cm^{-1} are present in the IR spectra of the obtained complex. The ^{1}H NMR spectra of the complex showed the sharp singlet at 6.07 ppm characteristic of the co-ordinated η^6-C_6H_6 ligand. The protons of phenantroline ligand resonated at 8.42 (dd H2, 9), 7.74 (dd H3, 8), 8.32 (dd H4, 7), 7.93 (s H5, 6). The protons of phenanthroline ligand are assigned as follows:

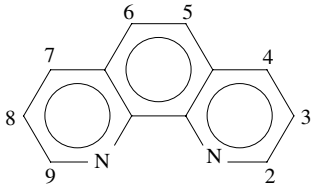

Crystal structures

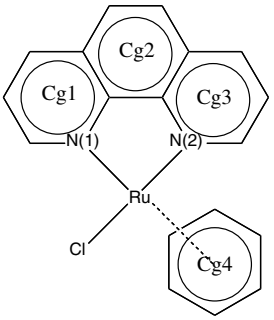

Fig. 2. Structural drawing of $[(C_6H_6)RuCl(1,10\text{-}C_{12}H_8N_2)_2]Cl$.

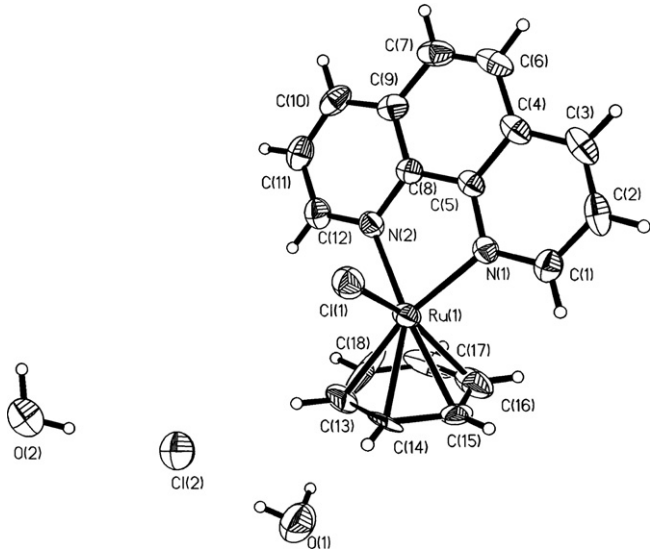

Fig. 1. ORTEP drawing of $[(C_6H_6)RuCl(1,10\text{-}C_{12}H_8N_2)_2]Cl \cdot 2H_2O$ with 50% probability thermal ellipsoids.

Table 3
Hydrogen bonds for $[(C_6H_6)RuCl(1,10\text{-}C_{12}H_8N_2)_2]Cl \cdot 2H_2O$ (Å and °)

D–H···A	*d*(D–H)	*d*(H···A)	*d*(D···A)	∠(DHA)
O(1)–H(1O)···Cl(2)	0.92	2.35	3.243(4)	165.1
O(1)–H(1P)···O(2)#1	1.02	1.91	2.905(5)	165.7
O(2)–H(2P)···Cl(2)	0.92	2.27	3.172(2)	166.9
O(2)–H(2O)···Cl(2)#2	0.99	2.20	3.187(4)	173.6
C(1)–H(1)···O(1)#3	0.93	2.54	3.447(4)	164.8
C(10)–H(10)···Cl(1)#4	0.93	2.74	3.626(4)	159.4
C(11)–H(11)···O(1)#5	0.93	2.53	3.254(5)	134.5
C(13)–H(13)···Cl(2)	0.93	2.82	3.660(5)	151.3
C(15)–H(15)···O(1)#3	0.93	2.58	3.308(6)	135.0
C(2)–H(2)···Cg1#6	0.93	3.39	3.342(6)	78.99
C(10)–H(10)···Cg1#7	0.93	3.19	3.475(7)	99.83
C(15)–H(15)···Cg4#4	0.93	3.32	3.471(6)	91.38

Symmetry transformations used to generate equivalent atoms: #1 $x-1, y, z$; #2 $-x+2, -y, -z$; #3 $-x, -y+1, -z$; #4 $-x+1, -y, -z+1$; #5 $-x+1, -y, -z$, #6 $-x, -y+1, -z+1$; #7 $-x, -y, -z+1$.
Aromatic ring numbering scheme according to Fig. 2.

Table 2
Selected bond lengths (Å) and angles (°) for $[(C_6H_6)RuCl(1,10\text{-}C_{12}H_8N_2)_2]Cl \cdot 2H_2O$

Bond lengths (Å)			Angles (°)		
	Experimental	Calculated		Experimental	Calculated
Ru(1)–N(2)	2.097(3)	2.130	N(1)–Ru(1)–N(2)	77.72(10)	77.40
Ru(1)–N(1)	2.107(3)	2.131	N(1)–Ru(1)–Cl(1)	86.68(8)	84.09
Ru(1)–Cl(1)	2.4153(10)	2.394	N(2)–Ru(1)–Cl(1)	83.38(8)	83.95
Ru(1)–C(13)	2.172(4)	2.258	N(2)–Ru(1)–C(13)	115.7(2)	114.12
Ru(1)–C(14)	2.165(5)	2.250	N(2)–Ru(1)–C(14)	149.5(2)	148.70
Ru(1)–C(15)	2.174(5)	2.266	N(2)–Ru(1)–C(15)	169.0(2)	168.47
Ru(1)–C(16)	2.150(5)	2.254	N(2)–Ru(1)–C(16)	132.8(3)	131.16
Ru(1)–C(17)	2.166(6)	2.289	N(2)–Ru(1)–C(17)	102.8(2)	102.87
Ru(1)–C(18)	2.162(5)	2.256	N(2)–Ru(1)–C(18)	95.62(19)	94.85
O(1)–H(10)	0.9155		N(1)–Ru(1)–C(13)	166.6(2)	167.96
O(1)–H(1P)	1.0171		N(1)–Ru(1)–C(14)	131.1(2)	131.78
O(2)–H(20)	0.9938		N(1)–Ru(1)–C(15)	102.17(17)	102.93
O(2)–H(2P)	0.9191		N(1)–Ru(1)–C(16)	92.69(17)	95.67
			N(1)–Ru(1)–C(17)	109.8(3)	113.24
			N(1)–Ru(1)–C(18)	146.4(4)	147.39
			C(17)–Ru(1)–Cl(1)	163.2(2)	162.26
			C(14)–Ru(1)–Cl(1)	88.14(15)	87.96
			C(16)–Ru(1)–C(13)	77.6(2)	77.55
			C(17)–Ru(1)–C(14)	78.6(2)	77.97
			C(18)–Ru(1)–C(15)	78.3(2)	77.68
			H(1O)–O(1)–H(1P)	100.1	
			H(2O)–O(2)–H(2P)	108.8	

3.1. Crystal structures

The $[(C_6H_6)RuCl(1,10\text{-}C_{12}H_8N_2)_2]Cl$ complex crystallises in the triclinic space group $P\bar{1}$. The molecular structure of the compound is shown in Fig. 1 (structural drawing of the complex is presented in Fig. 2). The selected bond lengths and angles are listed in Table 2. The benzene ring is disordered in two positions, molecules in both domains are coplanar and the second is rotated about 23° along axis linking ruthenium and benzene ring centroid.

The ruthenium atom is π-bonded to the benzene ring with an average Ru–C distance of 2.165(5) Å (range 2.150(5)–2.174(5) Å) whereas the distance between the ruthenium atom and the centroid of the ring is 1.685 Å and is consistent with those reported for the other Ru(II) η^6-arene complexes [3d,32,33]. The ruthenium atom is also directly co-ordinated to two nitrogen atom of phe-

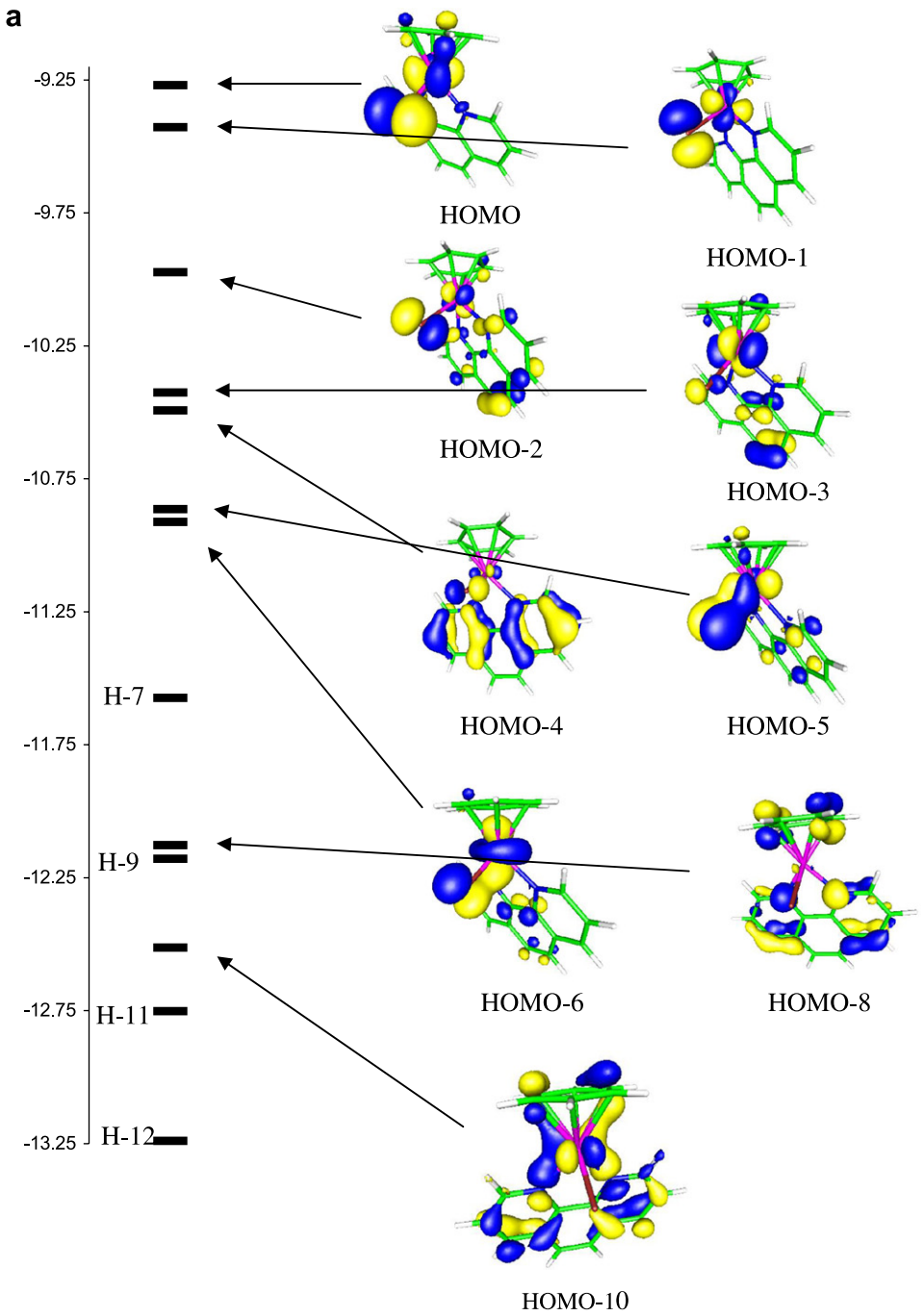

Fig. 3. The molecular orbital diagram (a) HOMO and (b) LUMO orbitals of $[(C_6H_6)RuCl(1,10\text{-}C_{12}H_8N_2)_2]Cl$.

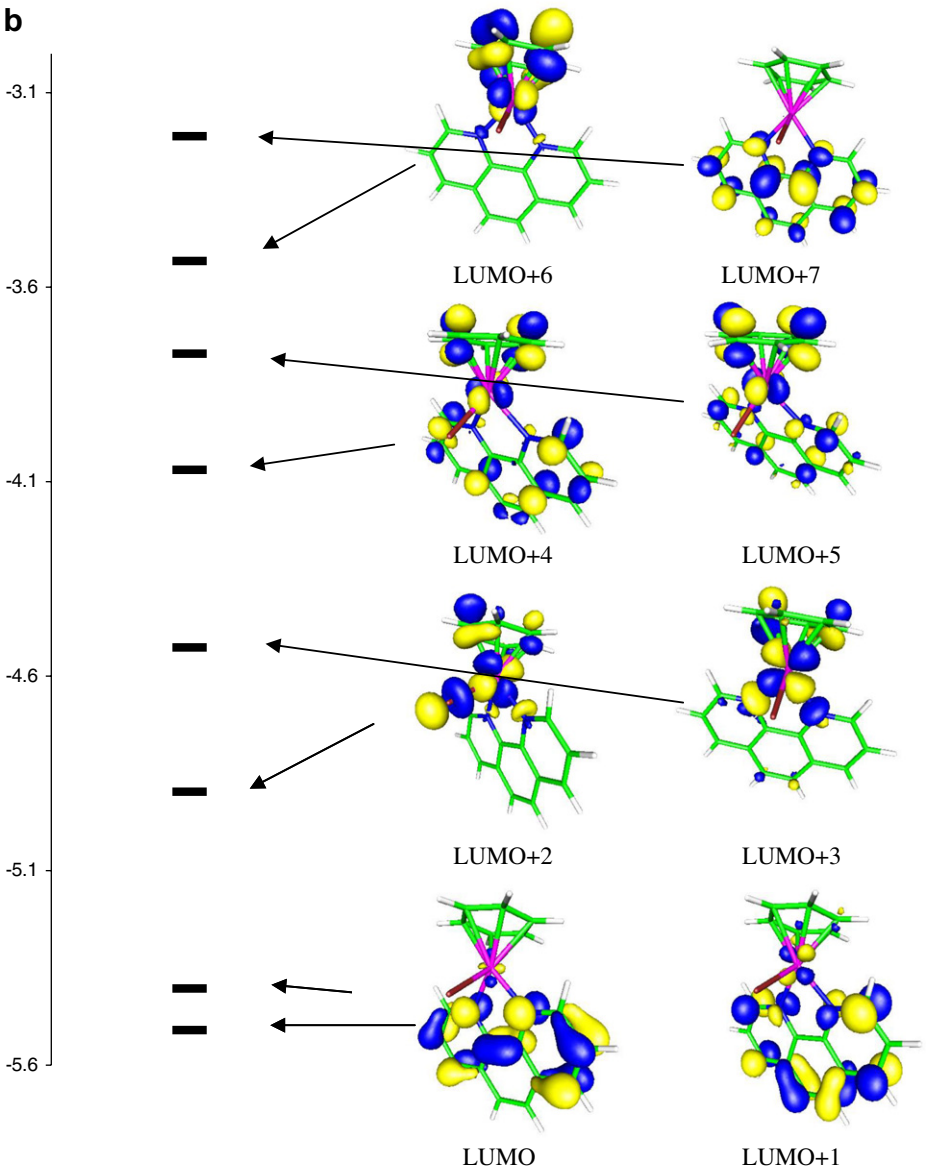

Fig. 3 (*continued*)

nanthroline ligand with an average distance of 2.102(3) and to chlorine ligand with the bond length of 2.415(10) Å. The angle of the chelating ligand (N(1)–Ru–(N2)) 77.72(10)° and the angles between phenanthroline nitrogen and chlorine ligand 86.68(8)° (N(1)–Ru–(Cl1)), 83.38(8)° (N(2)–Ru–(Cl1)) are close to those observed in the ruthenium arene compounds [34a–c]. The shortest Ru···Ru distance is equal to 7.000(1) Å (the second Ru atom obtained by $-x, -y+1, -z$ symmetry transformation).

The bond valences were computed as $v_{ij} = \exp[(R_{ij} - d_{ij})/b]$ [35–37], where R_{ij} is the bond valence parameter (in the formal sense the R_{ij} parameter value can be considered as an idealised single-bond length between i and j atoms). The R_{Ru-N}, $R_{Ru-\pi}$, R_{Ru-Cl} were taken as 1.656, 1.731 and 1.932 [38] respectively and b was taken as 0.37 [35]. The computed bond valences of ruthenium are $v_{Ru-N} = 0.296$ and 0.304 ($v_{Ru-phenanthroline} = 0.700$); $v_{Ru-\pi} = 1.132$; $v_{Ru-Cl} = 0.271$ v.u. (valence units) which means that Ru–π bond is almost four times stronger than other bonds, and the Ru–Cl bond is the weakest one. The valence sum rule states that the sum of the valences of the bonds formed by an atom is equal to the valence of the atom. Computed total valence of the Ru atom is 2.002 v.u. which agree with formal oxidation state and confirm the correctness of coordination sphere solution.

The six intermolecular hydrogen bond [39–41] linking the chlorine anion and water molecule O(2)–H(2O)···Cl(#2 $-x+2, -y, -z$) (D···A distance 3.187(4) Å, D–H···A angle 173.6°), two water molecules O(1)–H(1P)···O(2) (#1 $x-1, y, z$) (D···A distance 2.905(5) Å, D–H···A angle 165.7°), phenanthroline ligand and water C(1)–H(1)···O(1) (#3 $-x, -y+1, z$) (D···A distance 3.447(4) Å, D–H···A angle 164.8°), benzene and water mol-

ecule C(11)–H(11)···O(1) (#5 $-x+1$, $-y$, $-z$) (D···A distance 3.254(5) Å, D–H···A angle 134.5°), C(15)–H(15)···O(1) (#3 $-x,-y+1$, $-z$) (D···A distance 3.308(6) Å, D–H···A angle 135.0°) and chlorine ligand with benzene ring C(10)–H(10)···Cl(1) (#4 $-x+1$, $-y$, $-z+1$) are observed. Three other intramolecular weak hydrogen bond is presented in the structure of the complex: between arene C(13)–H(13) and Cl(2) (D···A distance 3.660(5) Å, D–H···A angle 151.3°) and between chlorine anion and water molecules O(1)–H(1O)···Cl(2) (D···A distance 3.243(4) Å, D–H···A angle 165.1°), O(2)–H(2P)···Cl(2) (D···A distance 3.172(2) Å, D–H···A angle 166.9°). Also C–H···π interactions (for details see Table 2) can be found in the molecule, and they can be classified, according to Desiraju and Steiner [39], as weak hydrogen bonds. The structure is stabilised by intermolecular stacking interactions between almost coplanar: (a) two phenanthroline rings systems (the second one obtained by # $-x$, $-y+1$, $-z+1$ symmetry transformation) with Cg1···Cg1#, Cg1···Cg2#, Cg2···Cg3#, Cg3···Cg2#, Cg3···Cg3# distances 3.736(5), 4.261(5), 3.524(5), 3.524(5), 3.617(5) Å and angles between Cg···Cg# vector and normal to planes Cg 27.7(3)°, 38.6(3)°, 21.3(3)°, 21.2(3)°, 24.1(3)° respectively (aromatic ring numbering scheme according to Fig. 2); (b) two phenanthroline rings systems (the second one obtained by # $-x+1$, $-y$, $-z+1$ symmetry transformation) with Cg2···Cg2#, Cg2···Cg3#, Cg3···Cg2# distances 3.871(5), 4.097(5), 4.097(5) Å and angles between Cg···Cg# vector and normal to planes Cg 31.9(3)°, 36.4(3)°, 37.8(3)° respectively; (c) two benzene rings (the second one obtained by # $-x$, $-y+1$, $-z$ symmetry transformation) with Cg4···Cg4# distance 3.92(4) Å and angle between Cg4···Cg4# vector and normal to planes Cg 32(2)° respectively (Table 3).

3.2. Geometry and electronic structure

The optimized geometry parameters for the complex are given in Table 2. The optimized bond distances and angles agree well with the experimental values. The largest differences were found for the ruthenium–benzene carbons distances. The shortening of the metal–benzene carbons distances is reproduced in the optimized structures. The bond lengths and angles obtained from both calculations are similar. The calculated Ru–benzene distance is 1.7613 Å.

The formal charge of ruthenium is +2 in this complex. The calculated charge on the ruthenium atom, obtained from natural population analysis, is close 0.793. The charge on the chloride ligand is higher than −1 (−0.518); the charge on phenanthroline nitrogen atoms is negative and amounts to −0.422. The HOMO–LUMO gap is 3.60 eV.

In Fig. 3 the molecular orbital diagram is presented with several HOMO (Fig. 3a) and LUMO (Fig. 3b) contours of molecular orbitals. The HOMO, HOMO − 1 and HOMO − 3 orbitals are d ruthenium type with the admixture of π chlorine orbitals. The HOMO − 2 is π chlorine orbital. The combinations of π chlorine and d metal orbitals create the HOMO − 5 and HOMO − 6 molecular orbitals of the complex. HOMO − 7 is the σ chlorine orbital. The phenanthroline ligand has a significant contribution in the HOMO − 4 and HOMO − 9 molecular orbitals. The lone pairs of phenanthroline nitrogen atoms are visible in HOMO − 10 and HOMO − 12.

The LUMO, LUMO + 1, LUMO + 4 and LUMO + 7 molecular orbitals are composed of phenanthroline rings. The ruthenium d orbitals hold shares in LUMO + 2, LUMO + 3 and LUMO + 5, LUMO + 6. The LUMO + 5 and LUMO + 6 MO have the antibonding contribution of the σ carbon orbitals from benzene ligand.

3.3. Electronic spectrum

The spin-allowed, singlet transitions were calculated with the TDDFT method. The experimental spectrum of the investigated complex shows bands at 449.4, 419.8, 324.0, 265.0, 232.6, 219.8 nm. The measured (solid line) and calculated (dashed and doted lines) electronic spectra are shown in Fig. 4. Each calculated transition in Fig. 4 was represented by a gaussian function with the height equal to the oscillator strength and width equal to 0.05. With the use of the TDDFT method 90, electronic transitions were calculated for $[(C_6H_6)RuCl(1,10\text{-}C_{12}H_8N_2)_2]^+$ using the DZVP with *f* functions basis set on ruthenium atom and the diffuse and polarization functions on the other atoms (doted line on Fig. 4.). Additionally, calculation of the electronic transitions was performed using the DZVP basis set on ruthenium atom and without the diffuse functions on the other atoms. The dashed line on the

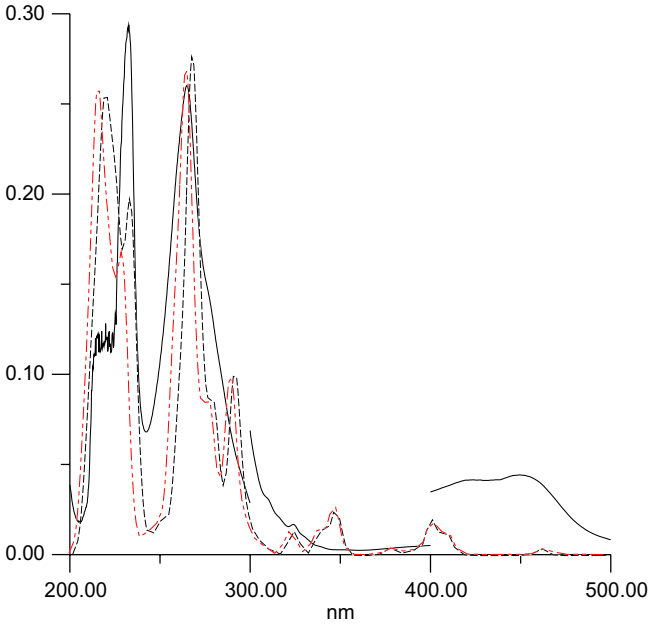

Fig. 4. UV–Vis spectrum of $[(C_6H_6)RuCl(1,10\text{-}C_{12}H_8N_2)_2]Cl$ (solid line – experimental; dashed and doted lines – calculated).

Table 4
Calculated electronic transitions for $[(C_6H_6)RuCl(1,10\text{-}C_{12}H_8N_2)_2]Cl$ with the TDDFT method

The most important orbital excitations		λ (nm)	E (eV)	f	Experimental λ (nm) (E (eV)) logε
$H(d+\pi_{Cl}) \rightarrow L+1(\pi^*_{Phen})$	$H-1(d+\pi_{Cl}) \rightarrow L+2(d)$	462.47	2.68	0.0038	449.4 (2.76)1.98
$H(d+\pi_{Cl}) \rightarrow L+2(d)$	$H-1(d+\pi_{Cl}) \rightarrow L+3(d)$	413.41	3.00	0.0009	
$H(d+\pi_{Cl}) \rightarrow L(\pi^*_{Phen})$	$H(d+\pi_{Cl}) \rightarrow L+3(d)$	398.26	3.11	0.0197	419.8 (2.95)1.97
$H-1(d+\pi_{Cl}) \rightarrow L+1(\pi^*_{Phen})$	$H-1(d+\pi_{Cl}) \rightarrow L+3(d)$	374.08	3.31	0.0041	
$H-2(\pi_{Cl}) \rightarrow L(\pi_{Phen})$	$H-2(\pi_{Cl}) \rightarrow L+2(d)$	343.00	3.61	0.0255	324.0 (3.83)4.88
$H-2(\pi_{Cl}) \rightarrow L+2(d)$	$H(d+\pi_{Cl}) \rightarrow L+3(d)$ $H-5(d+\pi_{Cl}) \rightarrow L+2(d)$	333.95	3.71	0.0135	
$H-4(\pi_{Phen}) \rightarrow L(d)$	$H-2(\pi_{Cl}) \rightarrow L+1(\pi^*_{Phen})$	318.45	3.89	0.0124	
$H-4(\pi_{Phen}) \rightarrow L+1(\pi^*_{Phen})$	$H(d) \rightarrow L+6(\pi^*_{benz})$	284.56	4.36	0.0779	265.0(4.68)5.47
$H-4(\pi_{Phen}) \rightarrow L+2(d)$	$H-5(d+\pi_{Cl}) \rightarrow L+3(d)$	282.15	4.34	0.0202	
$H-4(\pi_{Phen}) \rightarrow L+1(\pi^*_{Phen})$	$H-5(d+\pi_{Cl}) \rightarrow L+2(d)$	271.46	4.57	0.0666	
$H-6(d) \rightarrow L+1(\pi^*_{Phen})$	$H-6(d) \rightarrow L+3(d)$	264.01	4.70	0.0806	
$H-5(d+\pi_{Cl}) \rightarrow L(\pi^*_{Phen})$	$H-3(d) \rightarrow L+3(d)$	259.07	4.79	0.2369	
$H-5(d+\pi_{Cl}) \rightarrow L+2(d)$	$H-4(\pi_{Phen}) \rightarrow L+3(d)$	252.91	4.90	0.0499	
$H-3(d) \rightarrow L+4(\pi^*_{Phen})$	$H-8(\pi_{benz}) \rightarrow L+1(\pi^*_{Phen})$	224.23	5.53	0.1145	232.6(5.33)5.52
$H-8(\pi_{benz}) \rightarrow L(\pi^*_{Phen})$	$H-5(d+\pi_{Cl}) \rightarrow L+4(\pi^*_{Phen})$	221.94	5.59	0.0646	219.8(5.64)5.30
$H-4(\pi_{Phen}) \rightarrow L+4(\pi^*_{Phen})$	$H-10(n_{N(Phen)}) \rightarrow L(\pi^*_{Phen})$	216.13	5.74	0.0720	

Fig. 4. presents the obtained spectrum. The calculated spectra are in good agreement with the experimental one. The differences between the spectra calculated with and without diffuse functions are small, as it can be seen in the Fig. 4, and they are visible rather in intensities than in transitions energy.

As it can be seen from Table 4, we ascribe the first experimental band at 462.5 nm to the calculated transition at 449.4 nm with small oscillator strength. The next experimental band at 419.8 nm is assigned to the transition calculated at 398.3 nm. The transitions calculated between 343.0 and 318.5 nm are assigned to the band at 324.0 nm. The experimental band at 265.0 nm is attributed to the calculated excitations in the range of 284.6–252.9 nm. The calculated transition at 224.2 nm is ascribed to experimental data at 232.6 nm. The last experimental band at 219.8 nm is calculated between 221.9 and 216.1 nm.

The first two experimental bands consist of $d \rightarrow d$ (LF) and $d \rightarrow \pi^*_{Phen}$ (MLCT) transitions. The contribution of $d \rightarrow d$ excitation is visible in the experimental transition at 324.0 nm. In this band, the MLCT ($d \rightarrow \pi^*_{Phen}$), LMCT ($Cl \rightarrow d$) and LLCT ($\pi_{Phen} \rightarrow \pi^*_{Phen}$) transitions are observed. The next band at 265.0 nm is consisted from $Cl \rightarrow d$, $\pi_{Phen} \rightarrow d$, $\pi_{Phen} \rightarrow \pi^*_{Phen}$, $d \rightarrow \pi^*_{Phen}$ and $d \rightarrow \pi^*_{Phen}$ transitions. The $d \rightarrow \pi^*_{Phen}$ transition has a contribution in the bands at 232.6 and 219.8 nm. The $\pi_{benz} \rightarrow d$ (LMCT) excitation is visible in the band at 232.6 nm. The intraligand CT ($\pi_{Phen} \rightarrow \pi^*_{Phen}$, $\pi_{benz} \rightarrow \pi^*_{benz}$) transitions play a role in the band at 219.8 nm.

The phenanthroline ligand has a significant influence on the spectrum. The transitions with phenantroline (MLCT, LMCT, LLCT) occur in the whole spectrum apart from the low energy region over 400 nm (experimental bands at 462.5 and 419.8 nm). The differences between experimental and calculated UV–Vis spectra of the complex may follows that the known failure (only the transitions of energies smaller than the energy of HOMO orbital are well reproduced by this method) of the TDDFT method to describe CT transitions [42–46].

4. Supplementary material

CCDC 262846 contains the supplementary crystallographic data for this paper. These data can be obtained free of charge via http://www.ccdc.cam.ac.uk/conts/retrieving.html, or from the Cambridge Crystallographic Data Centre, 12 Union Road, Cambridge CB2 1EZ, UK; fax: (+44) 1223-336-033; or e-mail: deposit@ccdc.cam.ac.uk.

Acknowledgements

Crystallographic part was financed by funds allocated by the Ministry of Scientific Research and Information Technology to the Institute of General and Ecological Chemistry, Technical University of Łódź. The GAUSSIAN03 calculations were carried out in the Wrocław Centre for Networking and Supercomputing, WCSS, Wrocław, Poland under Calculational Grant No. 51/96.

References

[1] (a) H. Le Bozec, D. Touchard, P.H. Dixneuf, Adv. Organomet. Chem. 29 (1989) 163;
(b) R.M. Moriarty, U.S. Gill, Y.-Y. Ku, J. Organomet. Chem. 350 (1988) 157;
(c) R. Noyori, S. Hashiguchi, Acc. Chem. Res. 30 (1997) 97;
(d) M.A. Bennett, in: E.W. Abel, F.G.A. Stone, G. Wilkinson (Eds.), Comprehensive Organometallic Chemistry II, vol. 7, Pergamon Press, Oxford, 1995;
(e) M.A. Bennett, Coord. Chem. Rev. 166 (1997) 225.
[2] G. Winkhaus, H. Singer, J. Organomet. Chem. 7 (1967) 487.
[3] (a) I. de los Rios, M.J. Tenerio, M.A.J. Tenorio, M.C. Puerta, P. Valerga, J. Organomet. Chem. 525 (1996) 57;
(b) A. Schlüter, K. Bieber, W.S. Sheldrick, Inorg. Chim. Acta 340 (2002) 35;
(c) Y. Chen, M. Valentini, P.S. Pregosin, A. Albinati, Inorg. Chim. Acta 327 (2002) 4;
(d) A. Singh, N. Singh, D.S. Pandey, J. Organomet. Chem. 642 (2002) 48.
[4] (a) B. de Clercq, F. Verpoort, J. Mol. Catal. A: Chem. 180 (2002) 67;

(b) A. Kathó, D. Carmona, F. Viguri, C.D. Remacha, J. Kovács, F. Joó, L.A. Oro, J. Organomet. Chem. 593–594 (2000) 299;
(c) K. Mashima, K. Kusano, N. Sato, Y. Matsumura, K. Nozaki, H. Kumobayashi, N. Sayo, Y. Hori, T. Ishizaki, S. Akutagawa, H. Takaya, J. Org. Chem. 59 (1994) 3064;
(d) S. Hashiguchi, A. Fujii, J. Takehara, T. Ikariya, R. Noyori, J. Am. Chem. Soc. 117 (1995) 7562;
(e) A. Fujii, S. Hashiguchi, N. Uematsu, T. Ikariya, R. Noyori, J. Am. Chem. Soc. 118 (1996) 2521;
(f) A.W. Stumpf, E. Saive, A. Demonceau, A.F. Noels, J. Chem. Soc., Chem. Commun. (1995) 1127.

[5] (a) C.S. Allardyce, P.J. Dyson, D.J. Ellis, S.L. Heath, Chem. Commun. (2001) 1396;
(b) H. Chen, J.A. Parkinson, S. Parsons, R.A. Coxall, R.O. Gould, P.J. Sadler, J. Am. Chem. Soc. 124 (2002) 3064;
(c) R.E. Aird, J. Cummings, A.A. Ritchie, M. Muir, R.E. Morris, H. Chen, P.J. Sadler, D.I. Jodrell, Brit. J. Cancer 86 (2002) 1652;
(d) R.E. Morris, R.E. Aird, P. Del, S. Murdoch, H. Chen, J. Cummings, N.D. Hughes, S. Parsons, A. Parkin, G. Boyd, D.I. Jodrell, P.J. Sadler, J. Med. Chem. 44 (2001) 3616.

[6] S. Trofimenko, Chem. Rev. 93 (1993) 943.

[7] R. Mukherjee, Coord. Chem. Rev. 203 (2000) 151.

[8] G. La Monica, G.A. Ardizzoia, Prog. Inorg. Chem. 46 (1997) 151.

[9] A.P. Sadimenko, S.S. Basson, Coord. Chem. Rev. 147 (1996) 247.

[10] A.A. Batista, I.S. Thorburn, B.R. James, S.J. Rettig, R.G. Ball, in: Proc. 6th Int. Symp. Homogeneous Catalysis, Vancouver, Canada, 1988, p. 123.

[11] P.C. Hohenberg, W. Kohn, L.J. Sham, Adv. Quantum Chem. 21 (1990) 7.

[12] W. Kohn, A.D. Becke, R.G. Parr, J. Phys. Chem. 100 (1996) 12974.

[13] R.G. Parr, W. Yang, Ann. Rev. Phys. Chem. 46 (1995) 701.

[14] E.J. Baerends, O.V. Gritsenko, J. Phys. Chem. A 101 (1997) 5383.

[15] T. Ziegler, Chem. Rev. 91 (1991) 651.

[16] M.E. Casida, in: D.P. Chong (Ed.), Recent Advances in Density Functional Methods, vol. 1, World Scientific, Singapore, 1995.

[17] M.E. Casida, in: J.M. Seminario (Ed.), Recent developments and applications of modern density functional theory, Theoretical and Computational Chemistry, vol. 4, Elsevier, Amsterdam, 1996, p. 391.

[18] M.E. Casida, C. Jamorski, K.C. Casida, D.R. Salahub, J. Chem. Phys. 108 (1998) 4439.

[19] M.E. Casida, C. Jamorski, K.C. Casida, D.R. Salahub, J. Chem. Phys. 108 (1998) 4439.

[20] C. Adamo, V. Barone, Theor. Chem. Acta 105 (2000) 169.

[21] S.J.A. van Gisbergen, J.A. Groeneveld, A. Rosa, J.G. Snijders, E.J. Baerends, J. Phys. Chem. A 103 (1999) 6835.

[22] A. Rosa, E.J. Baerends, S.J.A. van Gisbergen, E. van Lenthe, J.A. Groeneveld, J.G. Snijders, J. Am. Chem. Soc. 121 (1999) 10356.

[23] M.A. Bennett, T.-N. Huang, T.W. Matheson, A.K. Smith, Inorg. Synth. 21 (1982) 74.

[24] M.J. Frisch, G.W. Trucks, H.B. Schlegel, G.E. Scuseria, M.A. Robb, J.R. Cheeseman, J.A. Montgomery Jr., T. Vreven, K.N. Kudin, J.C. Burant, J.M. Millam, S.S. Iyengar, J. Tomasi, V. Barone, B. Mennucci, M. Cossi, G. Scalmani, N. Rega, G.A. Petersson, H. Nakatsuji, M. Hada, M. Ehara, K. Toyota, R. Fukuda, J. Hasegawa, M. Ishida, T. Nakajima, Y. Honda, O. Kitao, H. Nakai, M. Klene, X. Li, J.E. Knox, H.P. Hratchian, J.B. Cross, C. Adamo, J. Jaramillo, R. Gomperts, R.E. Stratmann, O. Yazyev, A.J. Austin, R. Cammi, C. Pomelli, J.W. Ochterski, P.Y. Ayala, K. Morokuma, G.A. Voth, P. Salvador, J.J. Dannenberg, V.G. Zakrzewski, S. Dapprich, A.D. Daniels, M.C. Strain, O. Farkas, D.K. Malick, A.D. Rabuck, K. Raghavachari, J.B. Foresman, J.V. Ortiz, Q. Cui, A.G. Baboul, S. Clifford, J. Cioslowski, B.B. Stefanov, G. Liu, A. Liashenko, P. Piskorz, I. Komaromi, R.L. Martin, D.J. Fox, T. Keith, M.A. Al-Laham, C.Y. Peng, A. Nanayakkara, M. Challacombe, P.M.W. Gill, B. Johnson, W. Chen, M.W. Wong, C. Gonzalez, J.A. Pople, GAUSSIAN 03, Revision B.03, Gaussian, Inc., Pittsburgh PA, 2003.

[25] A.D. Becke, J. Chem. Phys. 98 (1993) 5648.

[26] C. Lee, W. Yang, R.G. Parr, Phys. Rev. B 37 (1988) 785.

[27] K. Eichkorn, F. Weigend, O. Treutler, R. Ahlrichs, Theor. Chim. Acc. 97 (1997) 119.

[28] A.D. Becke, J. Chem. Phys. 98 (1993) 5648.

[29] G.M. Sheldrick, Acta Crystallogr., Sect. A 46 (1990) 467.

[30] G.M. Sheldrick, SHELXL97. Program for the Solution and Refinement of Crystal Structures, University of Göttingen, Germany, 1997.

[31] G.M. Sheldrick, SHELXTL: release 4.1 for Siemens Crystallographic Research Systems, 1990.

[32] U. Beck, W. Hummel, H.B. Burgi, A. Ludi, Organometallics 6 (1993) 20.

[33] F.B. McCormick, D.D. Cox, W.B. Gleason, Organometallics 12 (1993) 610.

[34] (a) R. Tribo, J. Pons, R. Yanez, J.F. Piniella, A. Alvarez-Larena, J. Ros, Inorg. Chem. Commun. 3 (2000) 545;
(b) M. Jahncke, A. Neels, H. Stoeckli-Evans, G. Süss-Fink, J. Organomet. Chem. 561 (1998) 227;
(c) H. Kurosawa, H. Asano, Y. Miyaki, Inorg. Chim. Acta 270 (1998) 87.

[35] I.D. Brown, Acta Crystallogr., Sect. B 48 (1992) 553–572.

[36] I.D. Brown, Acta Crystallogr., Sect. B 53 (1997) 381–393.

[37] M. O'Keeffe, N.E. Brese, J. Am. Chem. Soc. 113 (1991) 3226–3229.

[38] J.G. Małecki, J.O. Dzigielewski, M. Jaworska, R. Kruszynski, T.J. Bartczak, Polyhedron 23 (5) (2004) 885–894.

[39] G.R. Desiraju, T. Steiner, The Weak Hydrogen Bond in Structural Chemistry and Biology, Oxford University Press, 1999.

[40] G.A. Jeffrey, W. Saenger, Hydrogen Bonding in Biological Structures, Springer-Verlag, 1994.

[41] R. Taylor, O. Kennard, J. Am. Chem. Soc. 104 (1982) 5063–5070.

[42] L. Bernaconi, M. Sprik, J. Hutter, Chem. Phys. Lett. 394 (2004) 141.

[43] S.R. Stoyanov, J.M. Villegas, D.P. Rillema, Inorg. Chem. Commun. 7 (2004) 838.

[44] M.E. Casida, C. Jamorski, K.C. Casida, D.R. Salahub, J. Chem. Phys. 108 (1998) 4439.

[45] D. Sundholm, Chem. Phys. Lett. 317 (2000) 545.

[46] D. Sundholm, Chem. Phys. Lett. 302 (1999) 480.